Development of a scanning angle total internal reflection Raman spectrometer

Kristopher J. McKee and Emily A. Smith

Articles you may be interested in

Development of a combined portable x-ray fluorescence and Raman spectrometer for in situ analysis
Rev. Sci. Instrum. **85**, 063113 (2014); 10.1063/1.4883188

Simultaneous detection of Raman scattering and near-infrared photoluminescence in one imaging microscope
Rev. Sci. Instrum. **83**, 063709 (2012); 10.1063/1.4731684

Optical cell for combinatorial in situ Raman spectroscopic measurements of hydrogen storage materials at high pressures and temperatures
Rev. Sci. Instrum. **82**, 033103 (2011); 10.1063/1.3558693

Construction of an integrated Raman- and angular-scattering microscope
Rev. Sci. Instrum. **80**, 044302 (2009); 10.1063/1.3124797

Multifunctional microscope for far-field and tip-enhanced Raman spectroscopy
Rev. Sci. Instrum. **77**, 023104 (2006); 10.1063/1.2162449

A WHOLE NEW LOOK FOR *PHYSICS TODAY* MAGAZINE COMING JANUARY 2016

1948　1964　1982　1985　1992　1997　2006　2012　2016

Development of a scanning angle total internal reflection Raman spectrometer

Kristopher J. McKee and Emily A. Smith[a)]
Ames Laboratory, U.S. Department of Energy, Ames, Iowa 50011-3111, USA and Department of Chemistry, Iowa State University, Ames, Iowa 50011-3111, USA

A scanning angle total internal reflection (SATIR) Raman spectrometer has been developed for measuring interfacial phenomena with chemical specificity and high axial resolution perpendicular to the interface. The instrument platform is an inverted optical microscope with added automated variable angle optics to control the angle of an incident laser on a prism/sample interface. These optics include two motorized translation stages, the first containing a focusing lens and the second a variable angle galvanometer mirror. The movement of all instrument components is coordinated to ensure that the same sample location and area are probed at each angle. At angles greater than the critical angle, an evanescent wave capable of producing Raman scatter is generated in the sample. The Raman scatter is collected by a microscope objective and directed to a dispersive spectrometer and charge-coupled device detector. In addition to the collected Raman scatter, light reflected from the prism/sample interface is collected to provide calibration parameters that enable modeling the distance over which the Raman scatter is collected for depth profiling measurements. The developed instrument has an incident angle range of 25.5°–75.5°, with a 0.05° angle resolution. Raman scatter can be collected from a ZnSe/organic interface over a range of roughly 35–180 nm. Far from the critical angle, the achieved axial resolution perpendicular to the focal plane is approximately 34 nm. This is roughly a 30-fold improvement relative to confocal Raman microscopy. © *2010 American Institute of Physics.* [doi:10.1063/1.3378682]

I. INTRODUCTION

A. Background

Total internal reflection (TIR) or attenuated total reflectance (ATR) Raman spectroscopy was first demonstrated as a surface sensitive vibrational technique by Ikeshoji in 1973.[1] Since its first validation, TIR Raman spectroscopy has been used to analyze a limited number of interfacial species at liquid-liquid, liquid-solid, and solid-solid interfaces.[2–8] The majority of these studies used a fixed angle of incident radiation; thus, collecting Raman scatter over a fixed distance from the interface. Typically, these distances range from 40 nm to 1 μm from the interface, depending on the instrument configuration employed.[4,5] A number of reports have shown the surface sensitivity of the TIR Raman technique in the analysis of polymer films and laminates of varying thickness.[5–8] Additionally, Bain and co-workers[8–10] have analyzed a variety of samples including wax layers on plant leaves, boundary lubricants at frictional contacts, phospholipid bilayers, and adsorbed species at a silica/water interface. There are a few reports where TIR Raman spectra have been measured using manual adjustment of the incident angle. For example, it has been shown that varying the angle of incident light at the sample interface can be used to measure the anisotropic refractive indices for nonlinear optical materials by determining the angle where maximum Raman scatter was collected.[11] Additionally, variable angle TIR Raman spectroscopy has been used to collect spectra of homogenous solutions and polymer laminates.[12–14] Up to now, the full scope of TIR Raman spectroscopy has not been utilized to perform high axial resolution depth profiling measurements. These measurements can be performed at ambient laboratory conditions, without obtrusive scanning probes and will provide chemical specific information. Numerous materials science and biological applications will benefit from these measurements, including studies of interfacial multilayers and biological films

B. Theory

An in-depth treatment of the theory of Raman scattering from evanescent waves is available in the literature.[15] Briefly, TIR occurs when light impinges on an interface between two materials of differing refractive indices, η_{prism} and η_{sample}, provided η_{prism} is greater than η_{sample} and the incident angle of light is greater than or equal to the critical angle, as determined by Snell's law. Under TIR, there is no net flux of photons across the interface; however, an evanescent wave is generated in the lower index of refraction medium as a result of the electromagnetic boundary conditions.[16] The evanescent wave travels parallel to the interface with a magnitude that decreases exponentially away from the interface. The depth at which the magnitude of the evanescent wave decreases to 1/e is known as the depth of penetration of the evanescent wave d_p. Since incoherent scattering is proportional to the square of the electric field, Raman scatter generated by an evanescent wave drops off twice as fast as the electric field. As a consequence, more than 98% of the Raman scatter is generated at a distance less than $d_p/2$.[8] The

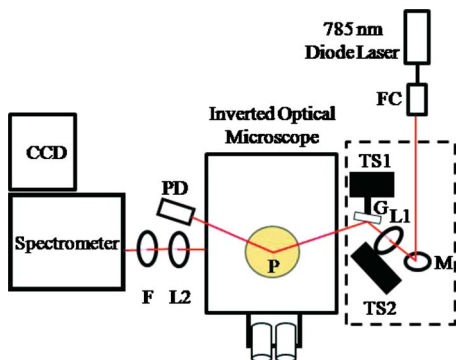a)Electronic mail: esmith1@iastate.edu.

FIG. 1. (Color online) Schematic from the top of the scanning angle TIR Raman microscope. The laser beam exits the fiber collimator and impinges on a mirror (M) oriented at 45° to direct the beam vertically through a focusing lens (F) to the galvanometer mirror (G), both of which are mounted on motorized translation stages (TSs). The galvanometer mirror directs the beam downward at an angle to the ZnSe prism (P)/sample interface. The light reflected from the interface is collected by a photodiode (PD) mounted on the opposite side of the prism. The Raman scatter generated in the sample is collected by a microscope objective and directed through a focusing lens (L) and a laser line filter (F) before entering the spectrometer equipped with a Near IR enhanced CCD. Optics in the dashed boxed are oriented perpendicular to the optical table and have been offset for clarity.

depth over which Raman scatter can be collected D_{RS} is calculated from the excitation wavelength (λ), refractive indices of the prism (η_{prism}) and sample (η_{sample}), and the angle of incidence (θ) using

$$D_{RS} = \frac{\lambda}{4\pi}[(\eta_{prism}^2 \sin^2 \theta) - \eta_{sample}^2]^{-1/2}. \quad (1)$$

As denoted in Eq. (1), it is possible to adjust the depth over which Raman scatter is collected by varying the angle of the incident light on the prism/sample interface. If a ZnSe prism is coupled to an organic solution and the incident angle can be controlled in 0.05° increments, spectra could theoretically be collected for a change in D_{RS} of 1 nm. Comparing this to confocal Raman microscopy, where the resolution obtained in the axis perpendicular to the focal plane is approximately 1000 nm,[17,18] several orders of magnitude improvement in the axial resolution is possible using TIR Raman spectroscopy.

The reflected light from a prism/sample interface can be modeled using Fresnel equations. For incident radiation of known polarization, the total reflected radiation R_T can be computed using Eq. (2). The fractions of the s- and p-polarized components of the laser are x_s and x_p; and the quantity of reflected s- and p-polarized radiation from the interface are R_s and R_p, respectively,

$$R_T = \frac{x_s R_s + x_p R_p}{2}. \quad (2)$$

II. EXPERIMENTAL

A. Instrument setup

A schematic of the scanning angle TIR (SATIR) Raman microscope is shown in Fig. 1. A 63 mW, 785 nm fiber coupled diode laser (Newport RLC785-63-50) fitted with a beam collimator is used as the excitation source. The beam is

directed vertically with the use of a mirror oriented 45° relative to the plane of the optical table to a focusing lens mounted on a motorized 450 mm translation stage (TS) (Zaber Technologies) and then a variable angle galvanometer (Cambridge Technology Model 6231) mounted on a second 300 mm motorized TS. Both TSs are mounted vertically with their direction of travel perpendicular to the plane of the optical table. The movement of the TSs, which have 0.5 μm resolution, and the galvanometer, which has 0.04° angular resolution, are controlled with an in-house developed application for LABVIEW 8.6 with a National Instruments I/O DAQ board (NI USB-6221). Coordinating the movement of the two TSs provides a constant optical path length between the focusing lens (L) and the prism/sample interface, and enables a facile match of the beam size and the microscope objective's field of view. The movement and focal length of the focusing lens can be changed depending on the desired laser spot size at the prism/sample interface. For all experiments, a 50.8 mm planoconvex lens with a focal length of 400 mm was used to provide a 1.1 mm diameter laser spot size at the sample. The galvanometer mirror directs the beam onto a 25.4 mm diameter hemispherical ZnSe chemical-vapor deposition prism ($\eta = 2.527$ at 785 nm) (ISP Optics) which is mounted in a custom sample holder on the stage of an inverted optical microscope (Nikon TE2000-U).

The mounted vertical position of the TSs on adjustable steel mounts can be altered to vary the achieved scanning incident angle range. For these experiments, the stages were mounted to provide an available incident angle range of 25.5°–75.5°. This incident angle range ensures that measurements could be taken below and above the critical angle for a variety of prism/sample interfaces. For example, if using a ZnSe prism, it would be possible to probe samples having a refractive index in the range of approximately 1.2–2.4.

Alignment of the laser spot at the prism/sample interface is aided by the use of a 12.5 mm complementary metal-oxide semiconductor (CMOS) camera mounted at the front port of the microscope. Using this camera, the position and area of the illuminated spot at the prism/sample interface are monitored at each angle. The generated Raman scatter is collected with a 10×, 0.22 numerical aperture (NA) objective lens (Nikon) and directed through the side port of the microscope where the light is focused onto an f/1.8i imaging spectrometer fitted with a holographic notch filter (Kaiser Optical Systems). Spectra are collected on a thermoelectrically cooled, back illuminated, deep depletion charge-coupled device (CCD) (Pixis 400BR, 1300×400 Princeton Instruments) controlled with the WINSPEC software package. A photodiode (PD) (Thor Laboratories SM1PD1A) fitted with a 1.0 optical density neutral density filter is mounted opposite of the galvanometer and is used to collect the light reflected from the prism/sample interface.

B. Sample analysis

1. Liquid sample

A liquid sample holder was custom-made from a 1.3 mm thick glass Petri dish. A circle roughly 19 mm in diameter was removed from the bottom of the dish and a 25.4 mm #1
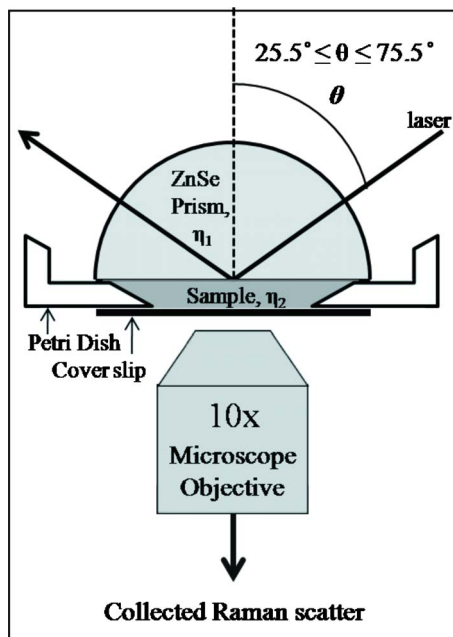
FIG. 2. (Color online) Schematic of the sample holder and TIR illumination geometry. The Raman scatter generated by the evanescent wave is collected by a 10×, 0.22 NA microscope objective.

glass cover slip was bonded to the bottom of the dish with optical adhesive (NOA 81, Norland Products) to create a sample well. To allow unimpeded passage of the incident and reflected radiation, the sides of the Petri dish were partially removed. A schematic of the sample configuration is shown in Fig. 2. In order to assemble the sample holder, 600 μl of 99% benzonitrile (Acros Organics) was added to the sample well, and the prism was mounted above the sample ensuring that no air bubbles were trapped at the interface. The sample assembly was then mounted on the stage of the optical microscope with the prism and sample centered above the collection optics. At each incident angle, a reflectivity measurement was recorded and a Raman spectrum acquired with an acquisition time of 10 min.

2. Polymer film

A polystyrene film was fabricated by drop coating 50 μl of a 20% (w/w) polystyrene (280 000M_w, Sigma Aldrich)/toluene (Fisher Scientific) solution directly onto the flat side of the ZnSe hemispherical prism. The solution was then allowed to dry under vacuum for 8 h. After the film dried, the prism was inverted and placed onto a custom made aluminum plate, with a 12 mm diameter opening to accommodate the objective and mounted on the stage of the microscope. Raman spectra were acquired at each angle with an acquisition time of 10 min.

C. Spectral data processing

All spectra were generated by averaging the central 100 vertical pixels of the CCD camera where the horizontal direction is the spectral dimension. The data was exported to Grams AI (Thermo Scientific) and baseline corrected to eliminate the broad but low background signal from the instrument optics. The data was then exported to IGORPRO 6

(Wavemetrics) for further analysis. The peak areas were determined using a Gaussian peak fitting algorithm. The reported data are the results for three replicate experiments. Algorithms were developed in IGORPRO to fit the reflectivity and Raman data sets to models based on the Fresnel and D$_{RS}$ calculations, as described in the following section.

III. RESULTS AND DISCUSSION

A. Reflectivity measurements

The computer controlled movement of the TSs and galvanometer shown in Fig. 1 can be used to vary the incident angle of the laser light on the prism/sample interface. The vertical displacement of the galvanometer and focusing lens are required to ensure the same area of the sample is being probed at each incident angle. The angle of incidence can be roughly measured using a protractor aligned on the microscope stage. However, further angle calibration is required for higher precision measurements. In order to calibrate the incident angle of the laser beam, the reflected light from a ZnSe/H$_2$O interface was recorded over a range of incident angles. This interface was chosen for angle calibration since the index of refraction of both materials is known at 785 nm, leaving the incident angle and laser polarization the only unknown parameters in Eq. (2). Using a laser power meter and a rotating polarizer, the measured laser polarization at the prism was 55% p-polarization and 45% s-polarization. Shown in Fig. 3(a) is the reflectivity data normalized to the highest measured reflected intensity and plotted along with theoretical reflectivity curves generated using Eq. (2). The instrument's incident angle measured using the microscope stage protractor does not match the calculated Fresnel values. After adjusting the data by $-1.33°$, a better match is achieved between the experimental and theoretical values [Fig. 3(b)].

After calibrating the instrument's incident angle, there is still considerable disparity between experiment and theory [Fig. 3(b) inset]. As mentioned in the experimental section, the laser spot diameter at the interface was 1.1 mm. This large beam diameter ensures that a large area of the sample is being probed by the laser beam. It also enables the use of lower photon fluxes per unit area and limits possible photodegradation of the sample. However, the fact that the beam is converging rather than collimated produces a distribution of incident angles at each instrument setting. The beam diameter was measured using a CMOS camera mounted at the front of the microscope to capture a visible image of the laser beam at the prism/sample interface allowing the range of probed angles to be back calculated. Using this measured diameter, the calculated incident angle spread is 2.9°. The beam diameter does not appreciably change as the instrument scans through the achievable incident angles.

If Eq. (2) is modified to account for an incident angle spread $\delta\theta$, a good fit between experiment and theory is obtained [Fig. 3(c)]. The instrument's angular resolution can be determined by varying the Fresnel fit to the higher and lower limit of the reflectivity data's standard deviation. The angular resolution of the instrument is 0.05° by this method.
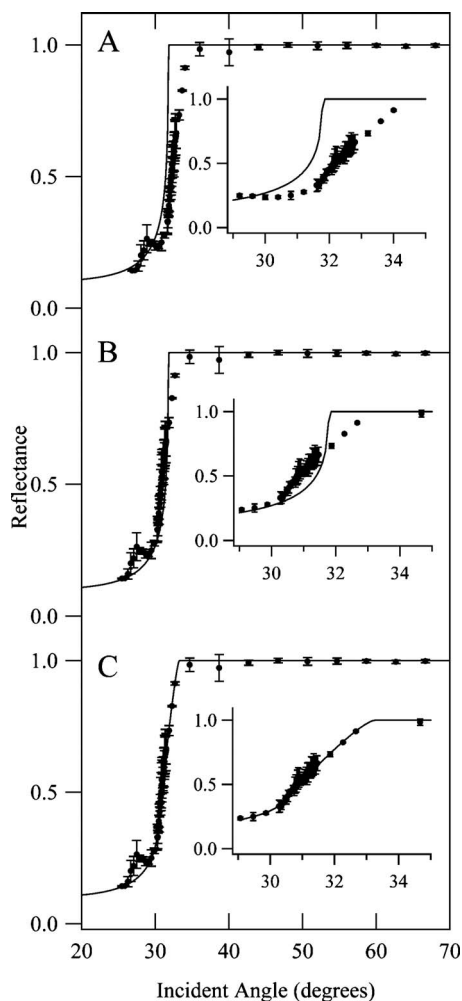
FIG. 3. Reflectance curve obtained at a ZnSe/H₂O interface (circles) with a 55% s-polarized and 45% p-polarized 785 nm laser. The solid line is the theoretical reflectance curve calculated using a Fresnel equation (a) prior to adjusting the incident angle of the data set; (b) after adjusting the incident angle of the data set; and (c) after introducing an incident angle spread into the theoretical Fresnel equation. The insets show an expanded view near the critical angle.
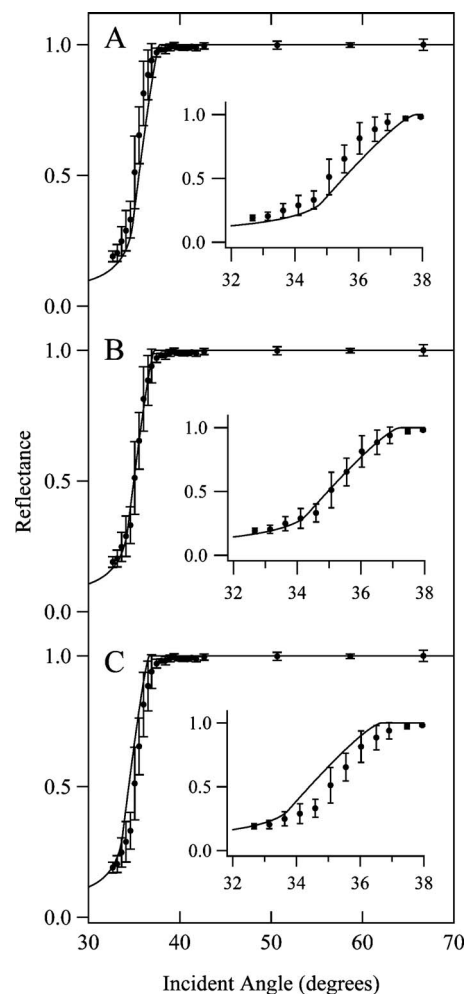

FIG. 4. Reflectance curve for a ZnSe/benzonitrile interface after angle adjustments were made (circles) and theoretical reflectance curves (line) with 785 nm incident radiation and (a) η_{sample}=1.492, (b) η_{sample}=1.472 which was found to be the best fit, and (c) η_{sample}=1.452. The insets show an expanded view near the critical angle.

The incident angle calibration and incident angle spread measured from the ZnSe/H₂O interface can be used to model the reflectivity data for interfaces where Raman scatter is to be collected. Prior to analyzing more complex samples, a model needs to be developed to correlate angle of incidence at the prism/sample interface with the depth over which Raman scatter is collected. A homogeneous solution of benzonitrile, a molecule with a high Raman scattering tensor, was chosen to develop this model. This model will have general applicability for other samples (e.g., polymer films and biofilms) provided the index of refraction of the sample is known from the literature or concurrently measured with the Raman scatter using reflectivity data, as outlined below.

As with most samples of interest that will be measured with scanning angle TIR Raman spectroscopy, the index of refraction of benzonitrile at 785 nm is not available in the literature. However, this value can be determined from the ZnSe/benzonitrile reflectivity data. Shown in Fig. 4 are the reflectivity values from a ZnSe/benzonitrile interface plotted

along with a theoretical reflectivity curve accounting for the calibration parameters determined from the ZnSe/H₂O interface. To illustrate the effect of η_{sample} on the theoretical reflectivity curve, the resulting curves using η_{sample} equal to 1.492, 1.472, and 1.452 are shown in Figs. 4(a)–4(c), respectively. The refractive index of benzonitrile was determined to be 1.472 by minimizing the residual between the experimental and theoretical data [Fig. 4(b)].

B. Raman spectra

In contrast to TIR fluorescence measurements where the signal level is high, the choice of TIR prism is critical for low signal TIR Raman measurements. The background values obtained in the Raman spectra using a glass (SF11) prism were between 5.74 and 17.5 counts/s throughout the fingerprint region of the spectrum (data not shown). The background included broad bands, likely due to fluorescence and scattering from the prism, with some minor contribution from other system optics. This background proved to be too high for practical TIR Raman measurements with this instrument. ZnSe, which has been used previously as in internal reflection element for ATR infrared and solid immersion lens
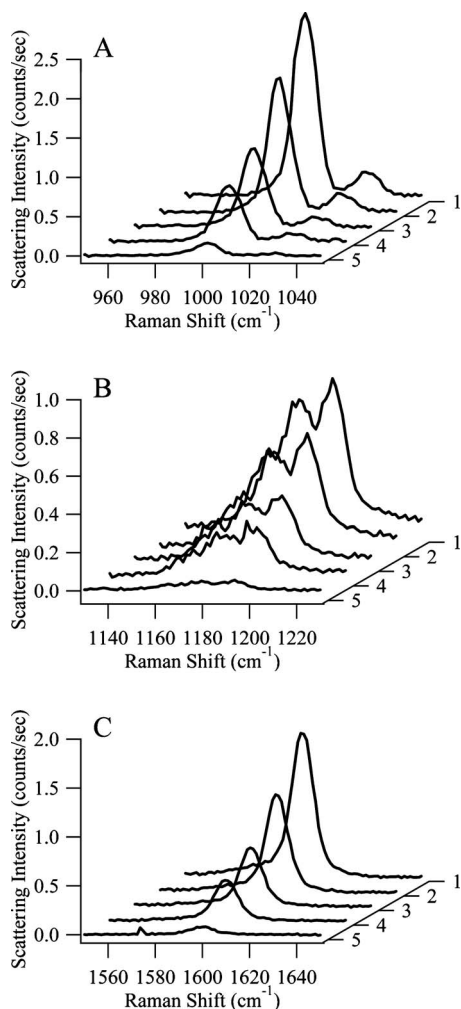
FIG. 5. TIR Raman spectra of benzonitrile at varying incident angles from (a) 950 to 1050 cm^{-1}, (b) 1130 to 1230 cm^{-1}, and (c) 1550 to 1650 cm^{-1}. The corresponding incident angles are (1) 37.47°, (2) 38.43°, (3) 41.31°, (4) 42.67°, and (5) 58.67°.

FIG. 6. (Right axis) Raman peak areas (circles) for the 1000 cm^{-1} benzonitrile peak and (left axis) D_{RS} curves (line) with (a) no angle spread and (b) $\pm 1.45°$ angle spread above and below the indicated x-axis value. The indicated error bar is the average uncertainty in peak area measured for all incident angles.

raman microspectroscopy,[19] was found to produce the lowest background signal of the prisms tested, between 1.14 and 15.19 counts/s, and was thus used for all subsequent Raman measurements. Additionally, the Raman spectrum of ZnSe only shows strong bands in the 200 to 500 cm^{-1} range which do not interfere with the main Raman modes of benzonitrile or the commonly analyzed modes for most organic analytes.

Raman spectra of benzonitrile at a ZnSe interface were recorded at incident angles ranging from 32.67° to 66.67°. The critical angle for a ZnSe/benzonitrile interface using the previously determined refractive index for benzonitrile is 35.74°. The spectra are shown in Fig. 5 for the most intense Raman peaks at select angles of incidence. The scattering intensity decreases as the incident angle increases further from the critical angle, as predicted by Eq. (1). The peak area at each incident angle was measured and is plotted in Fig. 6 (right axis) for the 1000 cm^{-1} ring breathing mode, which is the most intense benzonitrile peak. Also plotted in the same graph are the calculated D_{RS} values using Eq. (1). Figure 6(a) shows there is good agreement between the D_{RS} values as calculated with Eq. (1) and the measured values. However, the high peak intensities that are predicted by Eq. (1) are not
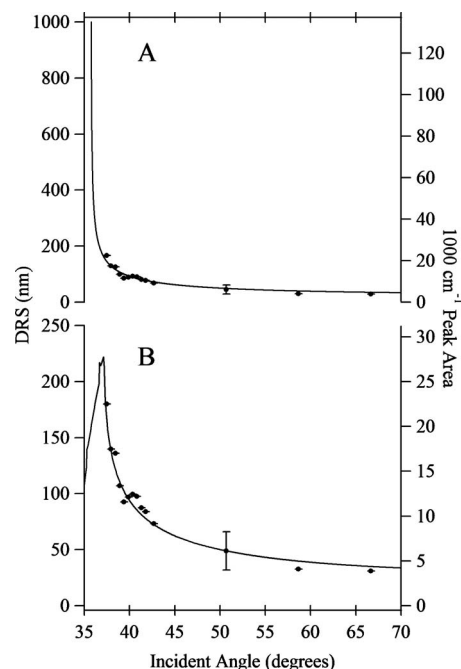
measured experimentally near the critical angle. As encountered with the Fresnel calculations, the D_{RS} equation must be modified to account for the converging excitation beam which results in an incident angle spread rather than a single incident angle. To account for the angle spread, the $\delta\theta$ term is entered into Eq. (1) and the sum is taken over all angles, where x is a resolution parameter that describes the number of divisions in $\delta\theta$. The equation for D_{RS} becomes

$$D_{RS} = \frac{\sum_{i=-x}^{x} \frac{\lambda}{4\pi} \left(\eta_{prism}^2 \sin^2\left[\theta + \left(\frac{\delta\theta}{2x} \right) i \right] - \eta_{sample}^2 \right)^{-1/2}}{2x+1}.$$

(3)

As shown in Fig. 6(b), the modified D_{RS} equation with a 2.9° angle spread provides a good fit to the experimental data. It was found that an x value of 1000 provided sufficient resolution to model the data. This model explains why the predicted Raman signals are not measured near the critical angle, as predicted by Eq. (1) without an angle spread.

As confirmed in Fig. 4(b), the incident beam is not entirely under TIR until the incident angle is above 37.20°. At this angle, the entirety of the beam is under TIR conditions and will be referred to as tTIR for "total" TIR. Spectra obtained at incident angles below tTIR will have some contribution from scattering caused by light transmitted through the ZnSe/benzonitrile interface (i.e., without surface sensitivity). The scatter from TIR cannot be differentiated from the scatter generated from the transmitted light; therefore, signal generated below the tTIR angle is not useful for depth profiling and is not modeled by Eqs. (1) or (3). For the ZnSe/benzonitrile interface under TIR conditions, the obtained Ra-

TABLE I. SATIR Raman instrument capabilities and measured performance for a ZnSe/benzonitrile interface.

	Angles	ΔD_{RS} (nm)	Percent change in Raman peak area (%)
Incident angle range	25.50°–75.50°		
Angular resolution	0.05°		
D_{RS} resolution	34 nm		
Close to tTIR	37.47°–37.95°	40	22.4
Far from tTIR	58.67°–66.67°	5	0.9

FIG. 7. (Right axis) Raman peak areas (circles) for the 1001 cm^{-1} polystyrene peak and (left axis) D_{RS} curves (line) with $\pm 1.45°$ angle spread above and below the indicated x-axis value. The indicated error bar is the average uncertainty in peak area measured for all incident angles.

man peak area can be correlated with the depth over which the Raman signal was collected using Fig. 6(b). With this interface and instrument settings, the D_{RS} versus incident angle curve is valid; however, the correlation of this curve to peak area will have to be performed for each peak in the Raman spectrum. This calibration is performed by fitting the experimentally determined peak area to the D_{RS} curve using a correlation factor that accounts for different scattering tensors and instrument response for each Raman active mode.

The D_{RS} range achieved for the ZnSe/benzonitrile interface from tTIR to the highest incident angle spanned from 35 to 180 nm. The smallest measured change in D_{RS} was 5 nm between 58.67° and 66.67°. This corresponds to a 0.9% change in Raman peak area. However, the average uncertainty in the Raman peak area was found to be 9.5%. This translates to a 34 nm uncertainty in measuring D_{RS} and is the axial resolution at this interface. A smaller angle change closer to the tTIR value from 37.47° to 37.95° corresponds to a 40 nm change in D_{RS}, and a 22.4% change in the peak area. A summary of the measured instrument performance is provided in Table I.

As a preliminary demonstration of the instrument's capabilities for measuring SATIR Raman spectra on a solid sample, spectra were collected at incident angles from 40.29° to 66.61° from a 56 ± 7 μm polystyrene film drop coated directly onto the prism. At these incident angles, the calculated D_{RS} values range from 37 to 190 nm. Figure 7 shows the correlation of the Raman peak areas for the 1001 cm^{-1} ring breathing mode to the calculated D_{RS} curve using Eq. (3).

IV. CONCLUSIONS

To our knowledge, this is the first report of an automated SATIR Raman spectrometer. The instrument and calibrations described herein provide the basis for chemical specific depth profile measurements at an interface with high axial resolution. Preliminary studies also show that, in addition to measurements in solution, the instrument is capable of col-
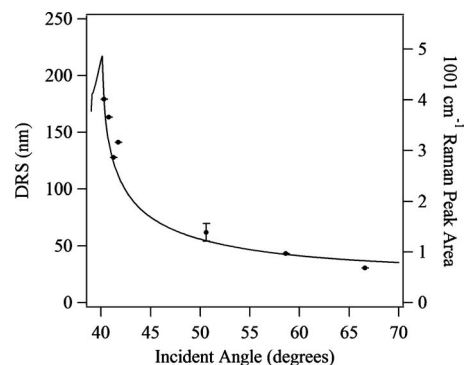
lecting TIR Raman spectra from thin solid films. The large incident angle range that can be scanned with the current setup, combined with the microscopy format, allows for the potential analysis of a multitude of liquid and solid samples. Current studies are focused on depth profiling measurements in polymer laminate films and biofilms.

[1] T. Ikeshoji, Y. Ono, and T. Mizuno, Appl. Opt. **12**, 2236 (1973).
[2] D. A. Beattie, M. L. Larsson, and A. R. Holmgren, Vib. Spectrosc. **41**, 198 (2006).
[3] K. Fujiwara and H. Watarai, Langmuir **19**, 2658 (2003).
[4] P. R. Greene and C. D. Bain, Colloids Surf., B **45**, 174 (2005).
[5] L. G. Tisinger and A. J. Sommer, Microsc. Microanal. **10**, 1318 (2004).
[6] R. Iwamoto, M. Miya, K. Ohta, and S. Mima, J. Am. Chem. Soc. **102**, 1212 (1980).
[7] R. Iwamoto, K. Ohta, M. Miya, and S. Mima, Appl. Spectrosc. **35**, 584 (1981).
[8] P. A. Greene and C. D. Bain, Spectroscopy Europe **16**, 8 (2004).
[9] C. Lee, H. Wacklin, and C. D. Bain, Soft Matter **5**, 568 (2009).
[10] E. Tyrode, M. W. Rutland, and C. D. Bain, J. Am. Chem. Soc. **130**, 17434 (2008).
[11] M. Yoshikawa, T. Gotoh, Y. Mori, M. Iwamoto, and H. Ishida, Appl. Phys. Lett. **64**, 2096 (1994).
[12] N. H. Fontaine and T. E. Furtak, J. Opt. Soc. Am. B **14**, 3342 (1997).
[13] N. H. Fontaine and T. E. Furtak, Phys. Rev. B **57**, 3807 (1998).
[14] R. Iwamoto, M. Miya, K. Ohta, and S. Mima, J. Chem. Phys. **74**, 4780 (1981).
[15] L. D'Hooge, J. M. Vigoureux, and C. J. Menu, J. Chem. Phys. **74**, 3639 (1981).
[16] W. M. Reichert, P. A. Suci, J. T. Ives, and J. D. Andrade, Appl. Spectrosc. **41**, 503 (1987).
[17] N. Everall, Spectroscopy **19**, 22 (2004).
[18] N. Everall, Spectroscopy **19**, 16 (2004).
[19] A. F. Sohn, L. G. Tisinger, and A. J. Sommer, Microsc. Microanal. **10**, 1316 (2004).